Chapter 1
Introduction to Neutron Physics

Yogesh S. Kashyap

1.1 Introduction

Neutrons have played a very important role in many of the scientific disciplines by providing important breakthrough discoveries, thereby contributing to modern scientific and industrial progress. Neutrons interact with all known fundamental forces in nature and, therefore, are a powerful tool for investigating domains of quantum mechanics, nuclear physics and cosmology, etc. Although the existence of neutrons was hypothesized by W. D. Harkins and E. Rutherford in the 1920s, however, its confirmation was provided in 1932 by James Chadwick, through meticulously planned experiments. The late discovery of neutron can be attributed to its similarity with the gamma rays, which too are emitted from the nucleus and show the property of charge neutrality. In fact, Irene curie and Fredric Joliot were first to notice the important property of this radiation—creating recoil protons while going through hydrogeneous media. However, it was Chadwick who realized and proved that the energy of the recoil proton can be explained only if the incoming radiation has a mass comparable to the proton mass and named it as neutrons. In particular, the discovery of neutrons provided an important impetus in the development of nuclear energy using nuclear reactors, which have in turn contributed to slowing down of emission of greenhouse gases in the earth's atmosphere. Medical isotopes produced through the use of nuclear transmutation by use of neutrons in many of nuclear reactors have played an equally important role in disease diagnosis, treatment of cancers, sterilization of medical equipment, etc. Similarly, low-energy neutrons are also useful in the treatment of certain types of tumours through the use of techniques such as boron neutron capture therapy (BNCT). In parallel, neutron imaging and neutron scattering have been developed into a very important tool in modern science and engineering, and owing to unique properties of neutrons, neutrons make an

Y. S. Kashyap (✉)
Technical Physics Division, Bhabha Atomic Research Center, Mumbai 400085, India
e-mail: yskashyap@barc.gov.in

D. K. Aswal et al. (eds.), *Neutron Imaging*,
https://doi.org/10.1007/978-981-16-6273-7_1

important complementary probe to X-rays. Due to nuclear-dependent scattering cross section, neutrons are complementary to X-rays in terms of isotopic sensitivity and have other unique properties such as large mean free path in matter and sensitivity to magnetism. We briefly mention some important reasons that makes neutron a unique probe in the non-destructive study of matter.

(i) As neutrons carry no charge, they have a large penetration depth in most materials. Hence, they are ideal for probing industrial samples, metallic objects, biological materials and in situ studies under externally applied conditions of pressure, temperature, etc. Similarly, the large penetration depth of neutrons permits us to study experimental processes within a chemical reaction vessel. Similarly, neutrons play important role in detection of light elements such as hydrogen, lithium and boron, due to their high neutron absorption properties. Neutrons are a unique and helpful probe for studying hydrogen storage materials, organic materials and biomolecular samples or polymers because they are highly sensitive to hydrogen.

(ii) Neutrons primarily interact with matter either of two ways: through the nuclear force or through the magnetic moment. Neutrons possess an intrinsic magnetic dipole moment, and hence, they are sensitive to magnetic fields (external or generated by unpaired electrons). Using a polarized neutron beam, the magnetic moment of a neutron may be used to examine the magnetic characteristics of materials. Furthermore, because neutron–nucleus interactions are spin dependent, neutrons may be used to investigate the spin dependence of nuclear forces and detect nuclear spin.

(iii) The wavelength of a neutron depends on its energy, and for thermal neutrons (~1 Å), it is roughly comparable to the distance between neighbouring atoms in materials. This makes them an ideal probe for determining atomic and molecular structures using neutron diffraction. The use of neutron diffraction to detect residual stress in metallic samples such as zirconium, aluminium, steel and others is a powerful and important tool for micro-strain studies inside the bulk of the materials.

(iv) The energies of thermal and cold neutrons are of the order of few meV or μeV. This energy is comparable to the energy required for thermally activated random motion of atoms in solids and liquids, and therefore, neutrons are ideal probe for studying such diffusive motion of atoms. Similarly, thermal vibrations of atoms in a crystal lattice (phonons) or oscillations of the magnetic moments (magnons) and a coupling between them can be easily probed using neutrons. Inelastic neutron scattering methods are also employed in neutron-based vibrational spectroscopy to explore the vibrational modes in molecules. As a result, neutrons are a perfect probe for studying these matter characteristics.

(v) As the neutron interacts with the nucleus in a quasi-random manner, lighter atoms such as $_1$H, $_3$Li and $_5$B can be easily detected even in the presence of heavier atoms, and nearby atoms may also be distinguished from each other. Moreover, one can also vary the contrast in certain samples using isotopic

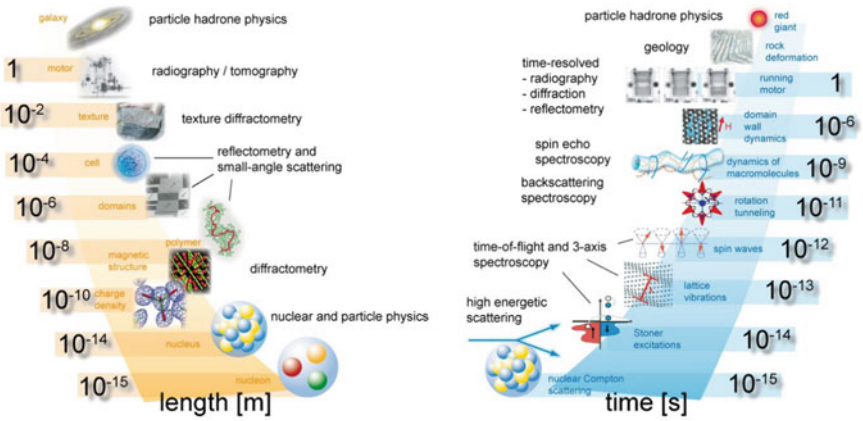

Fig. 1.1 Different length and timescales that can be probed using dedicated instruments using neutrons [1]

substitution techniques (e.g. deuterium for hydrogen, or one nickel isotope for another), and the same can also be used for study of complex ion formation process, partial structure factor determination and characterization of the internal structure of complex particles.

Figure 1.1 shows different neutron-based techniques and the length and time scales that they can probe. In the following section, we describe the fundamental properties of neutron and introduce the basic concepts in neutron imaging.

1.2 Properties of Neutrons

Neutrons are classified as hadrons, and they are subject to the strong nuclear force and belong to the family of baryons since they consist of three quarks. According to the standard model, the neutron is a neutral particle that is made of one up quark with charge +2/3 e and two down quarks with charge −1/3 e.

Proton, the other constituent of the nucleus, behaves almost identically under the influence of the short-range nuclear force (strong force) within the nucleus. Heisenberg proposed that the proton and neutron can be viewed as two quantum states of the same particle (charged and neutral) using the concept of isospin symmetry, and this formalism can be used to model the interactions of nucleons by the nuclear or weak forces.

Although there are many important properties of neutrons, we will focus on the following ones as they are most relevant for further development of the subject discussed in this book.

1.2.1 Neutron Mass

Chadwick obtained the value of the mass of the neutron using the following reaction:

$$^{11}_{5}B + ^{4}_{2}He \rightarrow ^{14}_{7}N + ^{1}_{0}n + Q \tag{1.1}$$

Upon substitution of all the atomic mass units in the above equation, Chadwick obtained the values of neutron mass as 1.0067 amu. The more precise value of the mass of neutron was made later by Bell and Elliot [2] from the following reaction:

$$^{1}_{1}H + ^{1}_{0}n \rightarrow ^{2}_{1}D + \gamma \tag{1.2}$$

The mass of the neutron obtained through the above measurement is 1.0008672 amu which was quite close to those obtained using a more precise measurement of 1.008664904(14) amu due to Bell and Elliot [3]. These measurements rule out any ambiguity that neutron could be composed of bound proton–electron pair, as postulated at the beginning of the twentieth century.

1.2.2 Neutron Charge

Since the beginning of discovery, zero electrical charge has been assigned to the neutron, as no measurable ionization is produced by neutrons in air. Experiments have been carried out by measuring neutron deflection as it passes through a transverse electrostatic field by Shull et al. [4] and gave an upper bound of the electric charge as 4×10^{-18} e (where e is the unit of electronic charge). Similar experiments were repeated at the Institute of Laue-Langevin in Grenoble, lateral displacement of neutrons was measured, and an upper limit $(-1.5 \pm 2.2) \times 10^{-20}$ e was obtained. More modern measurements have set an upper experimental limit on the charge of the neutron as -2×10^{-22} e reported by Olive [5]. In conclusion, therefore, one can safely use zero electrical charge as there is no experimental or theoretical evidence of any residual electrical charge on the neutrons.

1.2.3 Neutron Magnetic Dipole Moment

Even though the presence of an electric field has no effect on the neutron, studies have demonstrated that it may be significantly affected by an external magnetic field. The value of neutron magnetic moment was measured in a beautifully designed experiment by Alverez and Bloch [6] using the concept of nuclear magnetic resonance techniques and obtained the value which is quite close to the accepted value of −

1.91303 μ_n (in units of nuclear Bohr magneton). The negative sign emphasizes the fact that a neutron's magnetic moment and intrinsic spin point in opposite directions.

In the quark model of elementary particles, the neutron is made up of two "down" quarks of charge −1/3 e and one "up" quark of charge + 2/3 e. The magnetic moment of the neutron, therefore, arises due to the vector sum of the magnetic moments of the constituent quarks [7] and can also be calculated. Beg et al. [8] computed the ratio of intrinsic magnetic moments of neutron and proton to be −2/3, in good agreement with various experimental values to within 3%.

1.2.4 Neutron Spin

Neutrons have been found to behave like a Fermion, i.e. obey the Fermi–Dirac statistics, and have an intrinsic spin of 1/2. The interactions of the neutron's magnetic moment with an external magnetic field in a Stern–Gerlach type of experiments were used to confirm this hypothesis. In 1954, Sherwood et al. [9] employed neutrons in a Stern–Gerlach type of experimental set-up to record two spin states, thereby confirming that neutrons have an intrinsic spin of 1/2. It may be noted that neutron spin results in two refractive indices for neutrons in a magnetized media as demonstrated by Hughes and Burgy, who studied neutron reflection from ferromagnetic mirrors and observed angular distribution of reflection was consistent with spin 1/2 [10].

1.2.5 Neutron Lifetime

Unlike its counterpart proton, neutrons are not stable outside nuclei and undergo beta decay. These neutron lifetime measurement experiments can be broadly classified into two varieties, "bottle experiment" and "beam experiment". In a bottle experiment, ultra-cold neutrons are confined in a container, and undecayed neutrons are counted after a certain time has elapsed. In a beam experiment, researchers examine a stream of neutrons and count the number of protons produced by decay of neutrons. The neutron lifetime measurement has proved to be a difficult task primarily because that the data obtained with new experimental methods have been found to be in disagreement with earlier results [11]. There is nearly four standard deviations disagreement of 8.5 s between measurements of the neutron lifetime using the rate of neutron decay-producing protons measured in neutron beam experiments [12] (888.0 ± 2.0 s) and free neutron lifetime in bottle experiments [13] (879.4 ± 0.4 s). This lingering discrepancy is known as the "neutron lifetime puzzle", and it is still a matter of scientific debate; it is due to any unconsidered systematic effect or any new fundamental undiscovered physics.

1.2.6 Neutron Electric Dipole Moment

Although the neutrons have no electric charge, according to the standard model of particle physics, there exists a tiny separation of centres of the negative and positive charge distribution within the neutron, and this leads to a permanent electric dipole moment. Finding this neutron electric dipole moment would be a big breakthrough, in part because it could explain why matter in the cosmos did not simply vanish with antimatter at the beginning of time. It is worth noting that only if the centres of the negative and positive charge distributions inside the particle do not coincide, a finite electric dipole moment (EDM) can exist. So far, no neutron EDM has been found. The current best-measured limit for electric dipole moment is $(0.0 \pm 1.1) \times 10^{-26}$ e.cm[14]. Table 1.1 summarizes the discussion on various unique properties of neutrons.

1.3 Classification of Neutrons

As discussed earlier, neutron interacts with matter in a variety of ways, and the interaction probability is dependent on the energy of the neutron. Therefore, it is important to classify neutrons according to their kinetic energy. Moreover, neutrons can also be assigned a wavelength using the concept of wave–particle duality. The energy ranges described below are mainly concerned with differentiating how neutrons interact with materials for different applications.: nuclear fission, radiation shielding, neutron scattering, neutron imaging, etc. Note that the nomenclature and the energy ranges shown in the following definitions are not universal, and sometimes a group of energies can be recombined for ease of calculations (Table 1.2).

Table 1.1 List of some important properties of neutrons

S. No.	Important property	Value
1	Mass	1.00866491560(55) amu
2	Spin	1/2
3	Magnetic moment	$-1.91304273\ \mu_n$
4	Lifetime	885.7(8) s
5	Mean square charge radius	$-0.1161(22)$ fm^2
6	Electric charge	0 (experimental limits: $-2 \pm 8) \times 10^{-22}$ e)
7	Electric dipole moment	0 (experimental upper limit: 1.8×10^{-26} e.cm)
8	Electric polarizability	$12.5(2.5) \times 10^{-4}$ fm^3

Table 1.2 Classification of neutron according to the energy range [17, 18]

Neutrons type	Energy range	Wavelength [Å]
Ultra-cold	$\leq$ 300 neV	$\geq$ 500
Very cold	300 neV–0.12 meV	52.2–26.1
Cold	0.12–12 meV	26.1–2.6
Thermal	12–100 meV	2.6–0.9
Epithermal	100 meV–1 eV	0.9–0.28
Slow neutrons	1–10 eV	0.28–0.09
Resonance neutrons	10–300 eV	0.09–0.016
Intermediate	300 eV–1 MeV	
Fast	1–20 MeV	
High-energy neutrons	> 20 MeV	

1.3.1 Ultra-Cold Neutrons

Ultra-cold neutrons (UCN) have wavelengths greater than 500 Å ($E <= 300$ neV) and have several unique features. The first observation of the storage of ultra-cold neutrons was reported by Luschikov et al. [15]. This remarkable experiment was carried out at the Joint Institute for Nuclear Research at Dubna, USSR. It may be noted that for most materials, the optical potential of neutrons is less than ~300 neV, and, as a result, they are subjected to total external reflection at any angle of impact of the surface of most materials. This property enables neutrons to be stored in neutron tanks (or traps) to observe several fundamental characteristics [16]. The so-called trapped or bottled neutrons are mostly useful in understanding and addressing fundamental questions in physics, measurement of the neutron lifetime, gravitationally bound quantum states, neutron electric dipole moment, neutron beta decay studies, etc.

1.3.2 Very Cold Neutrons

Very cold neutrons have energies between ultra-cold neutrons and cold neutrons, typically corresponding to neV and sub-meV energies, i.e. from 300 neV–0.12 meV. These neutrons are obtained by use of D_2O ice, solid D_2 or CD_4 moderator cooled to 2–4 K, that is, a moderator at the temperature of liquid helium. In recent years, interest in the use of very cold neutrons has been increasing due to the possibility of obtaining better sensitivity in the detection of water in a fuel cell, water uptake in plant roots, etc.

1.3.3 Cold Neutrons

Cold neutrons have energies that are lower than thermal energies, often in the meV and sub-meV range., i.e. from 0.12 meV to 12 meV. The term, cold neutrons, refers to those neutrons whose wavelength exceeds the Bragg edge of polycrystalline beryllium (4 Å). Cold neutrons are produced in a neutron moderator using either liquid hydrogen or deuterium, supercooled gas, or solid (methane or ice) at temperatures ranging from 20 to 40 K. Cold neutrons are employed in a wide range of applications, including biomolecular structure investigations and neutron imaging, because they have a greater scattering and absorption cross section than hot neutrons. Moreover, because of high interaction cross sections, neutron optics such as mirrors, guides and polarizers can be more efficiently used to tailor the neutron beam properties for experiments.

1.3.4 Thermal Neutrons

Thermal neutrons are produced by slowing down more energetic neutrons in an uncooled moderator after they have been ejected from atomic nuclei during nuclear reactions such as fission, fusion and spallation. The high-energy neutrons constantly slow down and pick up energy, resulting in a Maxwellian distribution of neutron energies centred around the most likely energy (thermal energy). The term "thermal neutrons" refers to neutrons in a spectrum that are in thermodynamic equilibrium with moderator material at a temperature of 293 K, and corresponding mean energy is $E_{\text{th}} = 25.3$ meV. In thermal reactors, this region of the neutron's energy spectrum is the most important and useful part of the entire spectrum. A large number of instruments, such as those for neutron imaging and scattering, use thermal neutrons. Many research reactors also include so-called hot sources for use in short-wavelength applications, using a radiation-heated block of graphite at about 2000 K temperature. For a 2000 K temperature, the mean energy is $E_{\text{hot}} = 200$ meV.

1.3.5 Epithermal Neutrons

Epithermal refers to those neutrons which have energies higher than 100 meV, typically above 0.4 eV, the cadmium cut-off. Epithermal neutrons have a larger penetration depth as compared to thermal neutrons. Epithermal neutrons are preferred for application requiring large penetration depth such as boron neutron capture therapy and epithermal neutron imaging.

1.3.6 Resonance Neutrons

This usually refers to the energy range of 10–300 eV. This energy range corresponds to a nuclide's or element's resonance energy, usually uranium and its isotopes. As most of nuclei with which neutrons interact have a complex nuclear structures, it results in an enhanced interaction cross section or resonances in this energy range.

1.3.7 Intermediate Energy Neutrons

Typically, they have energy ranging from a few hundred electron volts (~100 eV) to one million electron volts (~1 MeV). Intermediate energy neutrons can be used to carry out neutron imaging applications, where greater depth of penetration is desirable.

1.3.8 Fast Neutrons

Generally, between 1 and 20 MeV, these are the energies of neutrons emitted by fission, accelerator and spallation sources. Another way of producing monoenergetic energy neutrons of 2.5 MeV and 14 MeV energy is to use D–D and D–T fusion reactions. In turn, this represents the upper limit of neutron radiobiology research and fundamental neutron interaction cross-section studies.

1.3.9 High-Energy Neutrons

These are neutrons having energy above 20 MeV. High-energy neutrons deliver a major portion of the dosage and effective dose in outer space, and they represent the area of greatest uncertainty in the biological effects of neutrons in space.

Figure 1.2 shows the Monte Carlo-simulated spectral intensity plot of neutrons as a function of energy for Intense Pulsed Neutron Source at Argonne National Laboratory for 100 K liquid methane for illustration purpose. The figure also shows a 293 K Maxwellian spectrum, which has a peak at an energy greater than the 100 K methane spectrum.

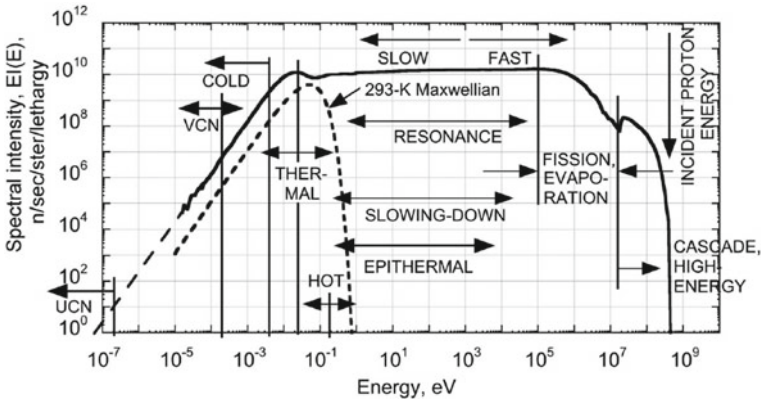

Fig. 1.2 Plot shows the spectrum of neutrons from 100 K liquid methane moderator of Intense Pulsed Neutron. *Source* at Argonne National Laboratory (reproduced from [19] with permission from Cambridge University Press)

1.4 Neutrons Matter Interaction

In the absence of charge and accompanying Coulomb interactions, neutrons interact with the nuclei of atoms by one or the both of the two mechanism: absorption and scattering (elastic scattering or inelastic scattering). Both of these interactions, absorption as well scattering, are highly dependent on neutron energy. Neutron absorption is due to neutron–nuclear interaction, and it usually leads to the release of gamma rays, charged particles, neutrons or fission fragments (Fig. 1.3). On the other hand, scattering could be due to nuclear interaction, magnetic interaction from unpaired electrons or Bragg scattering from the crystalline lattice and phonon and magnon excitation. As the wavelength and the energy of the thermal neutrons are comparable

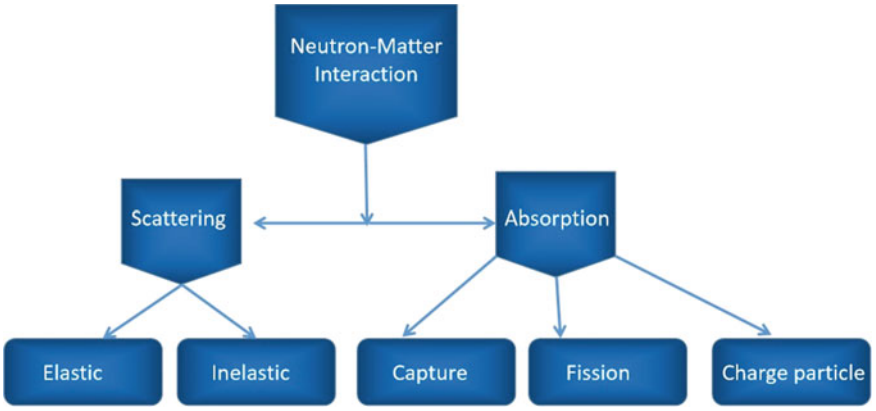

Fig. 1.3 Classification of scattering and absorption processes with neutrons

to lattice spacing and energy of various collective excitations in the crystals, they are useful in the study of crystal structures (including magnetic lattice), or phonon or magnon excitation. On the other hand for high-energy neutrons, nuclear interactions dominate over all other forms, and hence, they are more useful in the study of nuclear and particle physics, fast neutron activation analysis, etc.

The neutron matter interaction is best described through quantum mechanics in terms of wave function and probability density functions. This wave–particle duality is a fundamental idea behind quantum mechanics that describes the dynamics of subatomic particles, and therefore, one can sometimes refer to neutrons as particles and sometimes as waves. The parameter, namely scattering length (b), defines neutron interaction strength and is a phenomenological quantity. However, it cannot be calculated from fundamental principles, due to the complex nature of nuclear interactions.

The nuclear scattering lengths for the elements, as well as for individual isotopes, vary in a non-systematic manner with nucleus composition. The neutron scattering length of some elements is shown in Fig. 1.4.

As shown in Fig. 1.4, there is a markedly high difference in scattering length between hydrogen (^{1}H) and deuterium (^{2}H) ($b_H = -3.74$ fm and $b_D = 6.67$ fm). It should be noted that the scattering lengths of hydrogen and deuterium have distinct signs and hence used for contrast matching in many applications in soft matter research using neutron diffraction. Similarly, different isotopes of nickel show large variation in scattering length, and ^{58}Ni with the highest coherent scattering length is used for the fabrication of neutron optical elements such as neutron mirrors and guides. The quasi-random behaviour of scattering length of the neutron is in complete contrast with the more systematic scattering length of X-rays. It implies that neutrons can help in distinguishing isotopes or nearby elements in the periodic table.

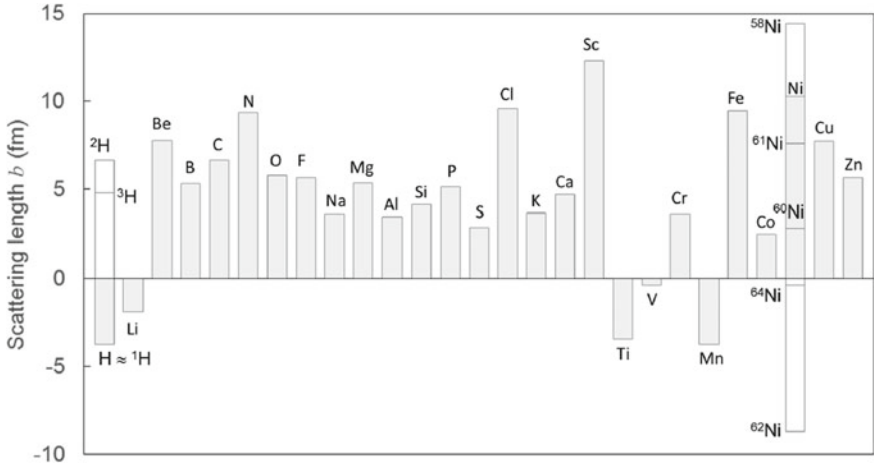

Fig. 1.4 Coherent bound scattering length variation of some elements for neutrons [20]

However, scattering lengths are not experimentally measurable parameters. Neutron scattering experiments measure the number of neutrons scattered by a sample according to the change in wave vector (Q) and the change in energy (E) of the neutron, described by the partial differential scattering cross section:

$$\frac{d^2\sigma_s}{\mathrm{d}\Omega \mathrm{d}E} = \frac{\text{no. of neutrons scattered per sec into d}\Omega \text{ in the energy range } [E,\ E + \mathrm{d}E]}{\mathrm{d}\Omega \mathrm{d}E \times \text{ incident neutron flux}} \tag{1.3}$$

The scattering intensity is divided by the neutron flux to ensure that σ is an intrinsic property, independent of the neutron flux at the particular experimental set-up. Integrating over all final energies, we reach the differential cross section

$$\frac{d\sigma_s}{\mathrm{d}\Omega} = \int \frac{d^2\sigma_s}{\mathrm{d}\Omega \mathrm{d}E} \mathrm{d}E \tag{1.4}$$

The total cross-section is found by a double integration, with dΩ as solid angle:

$$\sigma_s = \int \frac{d^2\sigma_s}{\mathrm{d}\Omega \mathrm{d}E} \mathrm{d}E \mathrm{d}\Omega \tag{1.5}$$

The neutron scattering cross section, σ_s, of a system is defined by its ability to scatter neutrons, and it has the unit of area. For a single nucleus, σ_s can now be seen as the effective area of the nucleus perpendicular to the neutron beam. The total cross section is a sum of two quantities: a term representing the probability of absorption by the nucleus (σ_a) and a term representing the probability of scattering by nucleus (σ_s). Figure 1.5 illustrates cross sections of some selected isotopes as a function of neutron energy in selected isotopes and hydrogen-rich plastic foils, showing that usually the cross section decreases as neutron energy increases.

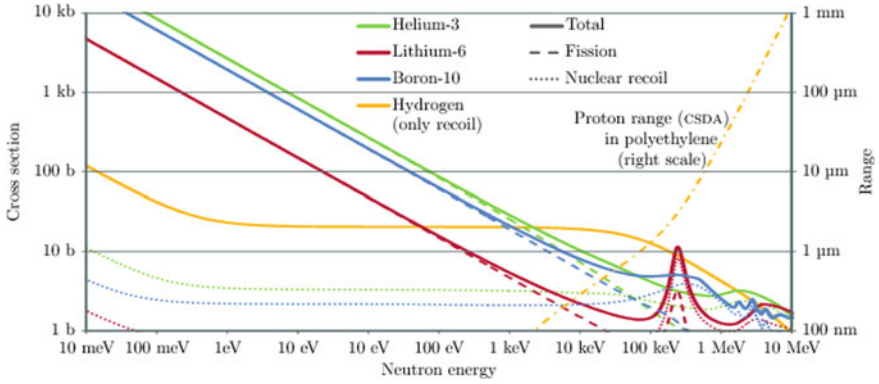

Fig. 1.5 Cross sections of various selected isotopes as a function of neutron energy and hydrogen-rich plastic foils [21]

In order to develop these ideas further, let us assume that neutron and matter interaction can be described by some finite range potential such that $V(r) = 0$ if $r > b$. Therefore, one needs to find out the solution of the time-independent Schrodinger equation,

$$\nabla^2\psi(\mathbf{r}) + K^2\psi(\mathbf{r}) = 0 \tag{1.6}$$

where

$$\begin{aligned} K^2(\boldsymbol{r}) &= \frac{2m}{\hbar^2}[E - V(\boldsymbol{r})]. \\ k^2(\boldsymbol{r}) &= \frac{2m}{\hbar^2}E. \end{aligned} \tag{1.7}$$

With the wave vector $\boldsymbol{k}$ outside the medium and wave vector $\boldsymbol{K}$ inside the medium (region of the potential), the incident particle being free, its wave function can be approximated by a plane wave

$$\psi = A\exp(-ik\cdot r) \tag{1.8}$$

where k is the incident wave vector and A is a normalization constant. After interaction with the matter medium, the amplitude of the outgoing wave can be approximated by

$$\psi = \frac{f(\theta,\phi)}{r}\exp(-ik\cdot r) \tag{1.9}$$

where $f(\theta,\ \phi)$ is the direction-dependent term and known as scattering amplitude. For completely isotopic scatter, needless to say, that it would be constant. The total wave function of the system consisting of the incident and scattered wave therefore can be represented as the sum of the incident and outgoing wave function as follows:

$$\psi = A\exp(-ik\cdot r) + \frac{f(\theta,\phi)}{r}\exp(-ik\cdot r) \tag{1.10}$$

Generally, we have the following relation between differential scattering cross section and scattering amplitude:

$$\frac{\mathrm{d}\sigma}{\mathrm{d}\Omega} = |f(\theta,\ \phi)|^2 \tag{1.11}$$

and total scattering cross section is given by:

$$\sigma_s = \int |f(\theta,\varphi)|^2\mathrm{d}\Omega \tag{1.12}$$

The total collision cross section, including both scattering and absorption, is given by the optical theorem

$$\sigma_t = \sigma_s + \sigma_a = \frac{4\pi}{k}\text{im}\left[f(0)\right] \tag{1.13}$$

The scattering amplitude can be expressed in terms of partial wave expansion. Consider a special case of scattering of the slow neutron from a fixed nucleus. When a neutron collides with this area, it scatters isotropically, that is, equally in all directions. Because the range of the nuclear interaction between the neutron and the nucleus is small in comparison with the wavelength of the neutron, the scattering is isotropic, and the nucleus appears to be a point scatterer. Generally, the scattering amplitude can be approximated by complex number, the scattering length b, which in general is complex quantity:

$$f(\theta,\, \phi) = -b + ikb^2 + O\left(k^2\right) \quad \text{where } b = b' - b'' \tag{1.14}$$

in which the k^2 term contains the effective range correction. When the higher-order partial waves are included, the k term also contains an anisotropic p-wave contribution.

Therefore, we can write

$$\sigma_s = 4\pi|b|^2\left(1 - 2kb'' + o\left(k^2\right)\right) \tag{1.15}$$

$$\sigma_a = \frac{4\pi}{k}b''\left(1 - 2kb'' + o\left(k^2\right)\right) \tag{1.16}$$

As it turns out that for most of the practical cases, $kb'' \ll 1$ and $b'' \ll b'$. Therefore, scattering and absorption cross sections can be as well approximated by the following simple expressions:

$$\begin{aligned} \sigma_s &= 4\pi|b|^2 \\ \sigma_a &= \frac{4\pi}{k}b'' \end{aligned} \tag{1.17}$$

In the above discussion, we have tacitly assumed that there are no resonances, which is usually true for thermal and cold neutron energies. In most practical cases, the interaction potential for s-wave scattering can be described in terms of scattering length b as follows (Fermi pseudopotential), which describes the effect of jth hard nuclei at the positions R_j.

$$V(\boldsymbol{r}) = \frac{2\pi\hbar^2}{m}\sum_j b_j\delta\left(\boldsymbol{r} - R_j\right) \tag{1.18}$$

Further, neutron scattering from several nuclei can be coherent or incoherent depending on whether the scattered waves from different scattering centres interfere or not. When considering elastic scattering from a crystal, the distinction between coherent and incoherent scattering becomes quite evident. Bragg peaks carry information about the relative positions of the atoms and results from coherent scattering of neutrons as a function of scattering angle. With the exception of isotopes with null nuclear spin (e.g. C, O), there are two possibilities in the interaction between a neutron and a nucleus: each atom's nuclear spin (I) couples with the neutron in either a parallel or anti-parallel manner. Since the neutron has a spin equal to 1/2, the spin of the ensemble, for each isotope, is $I + 1/2$ or $I - 1/2$ with the respective probabilities of $f_+ = I/2I + 1$ and $f_- = I/2I - 1$. Each interaction process corresponds to different scattering lengths, b_+ and b_-, respectively. We can define the average and the standard deviation that give, respectively, the "coherent" and "incoherent" scattering lengths:

$$\begin{aligned} b_c &= f_+ b_+ + f_- b_- \\ b_i &= \sqrt{\overline{b^2} - \overline{b}^2} \end{aligned} \tag{1.19}$$

Finally, we can define the neutron–nucleus interaction through the refractive index of the medium:

$$n(\boldsymbol{r}) = \frac{|\boldsymbol{K}(\boldsymbol{r})|}{|\boldsymbol{k}|} = \sqrt{1 - \frac{V(\boldsymbol{r})}{E}} \tag{1.20}$$

The mean interaction potential, or *optical potential*, for material is defined as follows:

$$\langle V(\boldsymbol{r}) \rangle = \overline{V} = \frac{2\pi\hbar^2}{m} b_c N \tag{1.21}$$

where N is the mean number of scattering nuclei per unit volume and $b_c = \langle b \rangle$ is the mean coherent scattering length. Accordingly, the complex index of refraction can be defined as follows:

$$n = \sqrt{1 - \frac{\overline{V}}{E}} = 1 - \frac{\lambda^2 N}{2\pi} \sqrt{b_C^2 - \left(\frac{\sigma_r}{2\lambda}\right)^2} + i \frac{\sigma_r N \lambda}{4\pi} = n_r + i n_i \tag{1.22}$$

The complex refraction index counts for absorption σ_a and incoherent scattering σ_i processes. $\sigma_r = \sigma_a + \sigma_i$ is the total reaction cross section per atom. If the imaginary part is small, therefore the index of refraction can be approximated as follows:

$$n = 1 - \frac{\lambda^2 N b_C}{2\pi} \tag{1.23}$$

1.5 Neutrons Imaging

Imaging science is a multidisciplinary field where two/three-dimensional pictorial distribution of certain object property is obtained. The most often useful property is the attenuation of the incoming radiation, as usually done in medical diagnostics, where X-ray radiography or a CT scan gives differential attenuation of the X-ray through the bones or tissues. These techniques work on extracting the relevant properties such as absorption coefficients which depend on the interaction of incoming radiation with the matter. Neutron imaging refers to a group of non-destructive testing methods, which exploit the transmission of neutrons through materials to probe the internal structure of objects, magnetic field distribution, etc. Owing to the large penetration depth in various materials, the development of neutron imaging started soon after the nuclear research reactor started operating. Only three years after the neutron was discovered, Hartmut Kallmann and Ernst Kuhn pioneered neutron imaging. Significant efforts by Thewlis marked the beginning of neutron imaging towards practical applications when he demonstrated it by utilizing a neutron beam from the British Experimental Pile (BEPO) reactor at Harwell. Initially, neutron imaging was carried out on the instruments used for neutron diffraction studies; however, it was soon realized that limited flux and small beam size did not permit the use of neutron for any practical sample. However, after J. P. Barton pioneered the divergent type of neutron collimators, leading to improved neutron flux and a larger field of view, thereby ushering a new era in the development of neutron imaging. Dr. W. L. Whittemore was the driving force behind the SNT-TC-1A personnel certification standard, which was first published in 1974 under the auspices of the American Society for Nondestructive Testing (ASNT). Until the 1990s, neutron imaging was carried out using film-based techniques, and hence, neutron radiography (two dimensional) was the only technique available to researchers. Since then, detection methods have improved drastically: digital neutron detectors and fast data acquisition and processing systems have been introduced, and neutron tomography has been implemented on most of the neutron imaging facilities. Moreover, introduction of new neutron optics like neutron guides and mirrors has also contributed to increased neutron flux at the sample positions. As a result of these innovations, and owing to the introduction of new imaging modalities, different from the conventional attenuation contrasts, new and challenging application fields have been established. Figure 1.6 summarizes different types of neutron imaging modalities along with the length scale probed by each one of them.

Broadly speaking, the current and the field of neutron imaging can be classified into four following major groups.

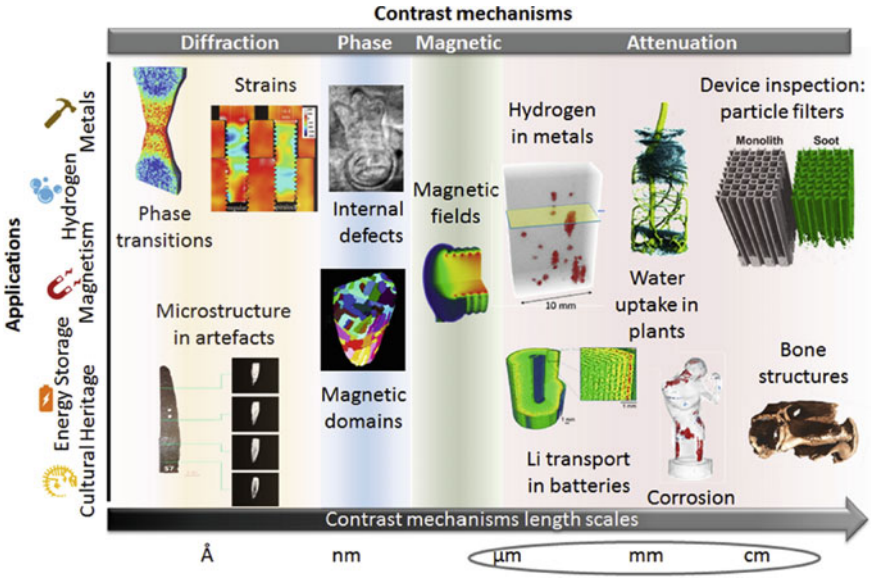

Fig. 1.6 Different contrast mechanism in neutron imaging (reproduced from [22] © 2018 Elsevier Ltd., with permission from Elsevier)

1.5.1 Attenuation-Based Neutron Imaging

This is the oldest scheme of neutron imaging, where an area detector (digital or film) measures the neutron beam transmission after it traverses through the object. The attenuation of the neutron beam can be easily modelled through Lambert–Beer law, which is given as $I = I_0 \exp(-\mu x)$, where μ is the neutron beam attenuation coefficient and includes all the ways neutrons beam is removed out of the path, due to various interaction mechanisms. This technique works best for those materials which have higher neutron absorption or incoherent scattering cross section. Another primary use of neutrons is in the structural investigation of high atomic number elements, where the X-ray fails to reveal internal or hidden details of the sample.

It may be noted that hydrogen (^{1}H) has the highest incoherent cross section, and therefore, this technique finds application where hydrogen detection or quantification is of primary concern. Moreover, one can collect the radiographs at different rotation angle, and complete three-dimensional distribution of the elements can be easily mapped. Figure 1.7 shows the three-dimensional distribution of hydrogen in the Zr alloy coupons, mapped using three-dimensional neutron tomography. The hydrogen concentrations were determined through use of calibrated samples.

As neutrons can penetrate in the metallic materials to larger depths, neutron radiography has also been widely used to map two-dimensional flow fields inside the metallic pipes as shown in Fig. 1.8.

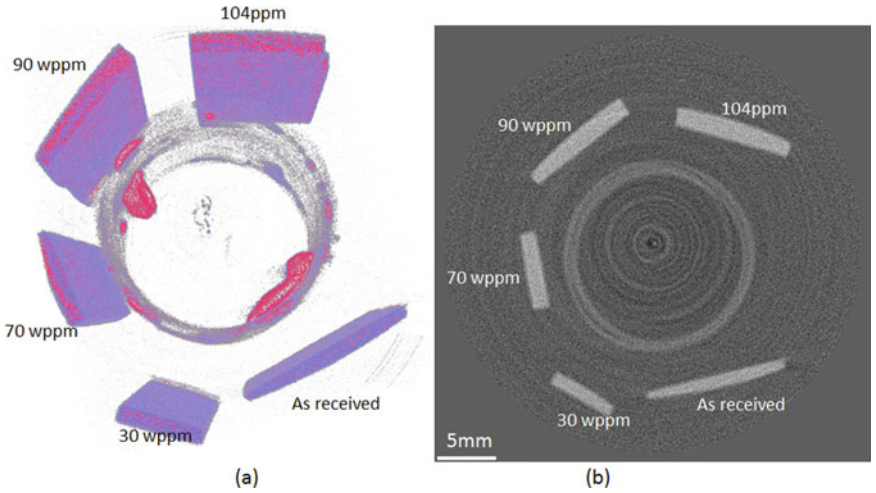

Fig. 1.7 Hydrogen distribution in Zr alloy using neutron tomography (reproduced from [23] © 2018, with permission from Elsevier)

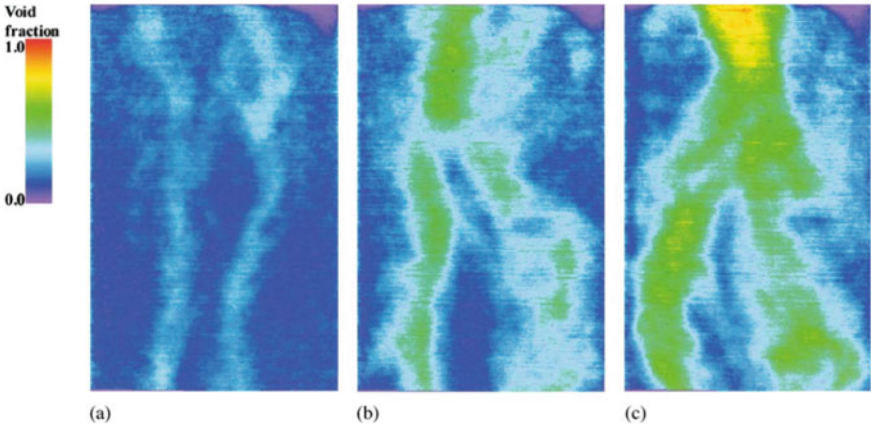

Fig. 1.8 Time-averaged void fraction profile taken by high frame rate neutron radiography (500 fps) for different gas flow rate. **a** $j_g = 1.4$ cm/s. **b** $j_g = 3.9$ cm/s. **c** $j_g = 12.3$ cm/s (reproduced from [24] © 2004 with permission from Elsevier)

The conventional neutron radiography also finds application in mapping the distribution of other elements such as lithium (Li-6), boron (B-10), cadmium (Cd-113) and gadolinium (Gd-157), as these elements have very large neutron absorption cross section. Figure 1.9 shows the dynamic neutron radiography was used to investigate lithium dendrite development during battery cycling. It shows dynamic distribution of lithium from the anode to cathode during charging and discharging cycles, induced by the internal short circuit due to lithium dendrite growth.

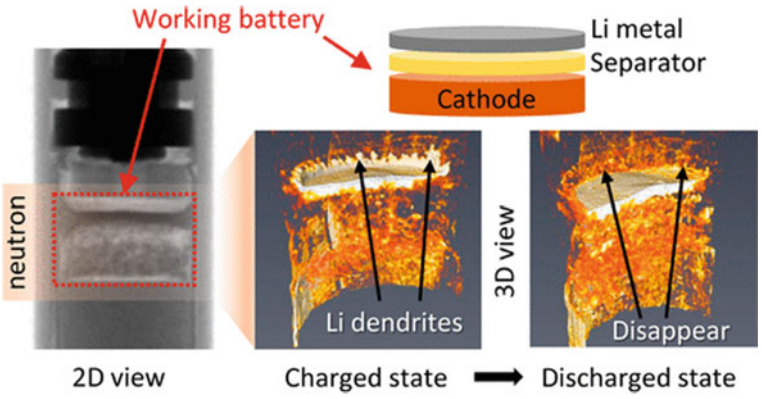

Fig. 1.9 Lithium distribution using in-operando neutron imaging (reproduced from [25] Copyright © 2019, with permission from American Chemical Society)

1.5.2 Phase Contrast Neutron Imaging

Conventional neutron-based imaging is based on so-called geometrical or ray optics. However, as neutron can also be treated as waves, we can associate a phase to the neutron wave, in analogy with the electromagnetic waves. This approach opens another avenue, namely the phase-based imaging techniques to study materials with low attenuation cross section, wherein the conventional attenuation-based imaging fails to reveal details within the sample under investigation. As the phase contrast effects are observed along with attenuation-based images, even the conventional neutron radiography improves in terms of detection sensitivity. A variety of interferometric and non-interferometric phase contrast techniques have been developed to measure either the slope of the phase or the curvature of the phase. Figure 1.10 shows an example of propagation-based phase contrast imaging using neutrons, and it clearly brings out the advantage of phase-based detection over the absorption-based one. Over the years, more sophisticated approaches which use crystal optics and near-field grating have also been developed to overcome the stringent requirement on the coherence as demanded by the propagation-based phase contrast technique. Another advantage of these phase contrast approaches is that we can obtain absorption, phase contrast and small-angle scatter contrast images from the same data set. The small-angle scatter contrast in these imaging modalities arises due to the presence of unresolved structures or structural inhomogeneities, below the point spread function of the system. Figure 1.11 shows tomographic reconstruction for a sample consisting of lead (black) and titanium (white) rods using grating-based neutron phase contrast imaging technique, showing the excellent sensitivity of the neutron phase contrast imaging in detection of materials with low neutron absorption cross section.

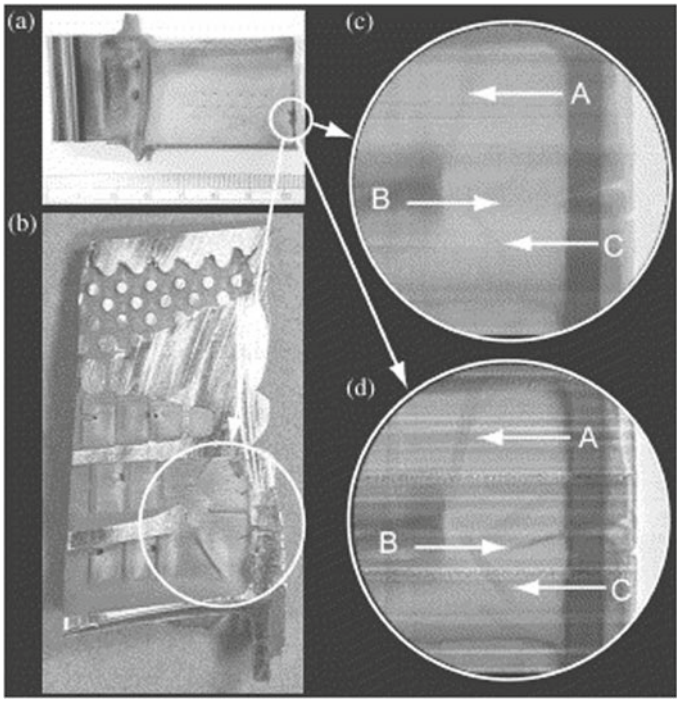

Fig. 1.10 **a** Encircled part of turbine blade was inspected for cracks, **b** destructive inspection of the turbine blade, **c** absorption-based neutron radiography, **d** phase contrast imaging of the same. The faint crack lines in **c** labelled with arrows *A*, *B* and *C* are greatly enhanced by phase contrast (reproduced from [26] © 2004, with permission from Elsevier)

1.5.3 Polarized Neutron Imaging

As discussed previously, although the neutron has zero electric charge, it does have a nonzero negative magnetic moment. The negative value of the magnetic moment implies that it is anti-parallel to spin angular momentum. This makes it possible for neutrons to interact with the magnetic moments of the atoms and, therefore, is used to study the detailed magnetic ordering in the solid materials. However, another application of neutron magnetic moment could be to obtain the spatial distribution of magnetic fields inside superconductors, visualization of DC or AC magnetic fields. Imaging with polarized neutrons is an important non-destructive technique to obtain the localized distribution of magnetic fields. For the polarized neutron imaging, a well-defined polarized neutron beam is initially selected using a supermirror or He^3-based polarizer. As the polarized neutron beam interacts with magnetic field of interest, the polarization vector undergoes precession, and the precession angle of the neutron polarization vector can be measured using an analyser. When used in combination of two-dimensional imaging detectors, and suitable data processing algorithm, the precession angles can be used to map the magnetic field direction

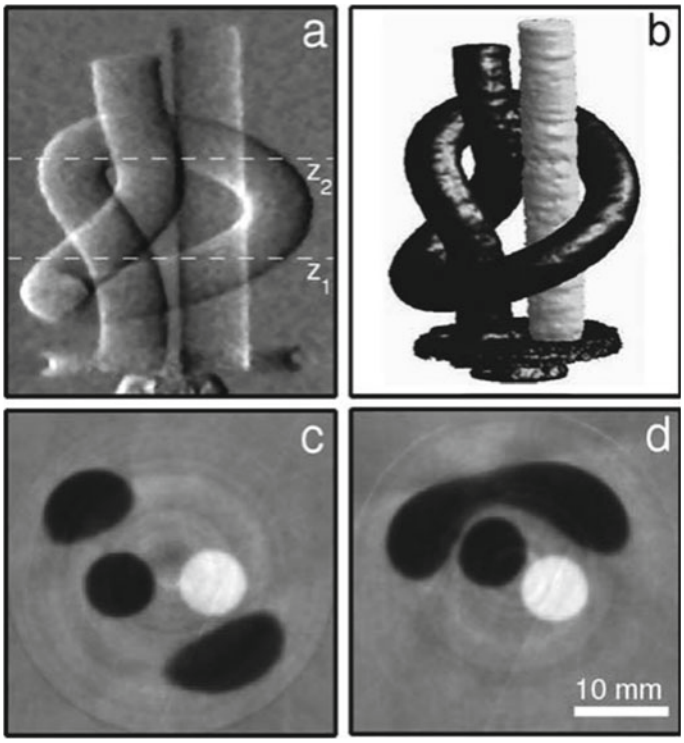

Fig. 1.11 Projection images and tomographic reconstruction of a sample made up of 6.35 mm diameter lead (black) and titanium (white) rods. **a** Image of a differential phase contrast projection. **b** A three-dimensional depiction of the sample's recovered coherent scattering length distribution. **c**, **d** two (out of 512) reconstructed tomographic slices (reprinted from [27] © 2006 with permission from the American Physical Society)

within the sample or given region of interest. The technique has been used to visualize modest magnetic fields (a few mT) with a low spatial resolution (100 μm) as shown in Fig. 1.12. In order to quantify the field integrals, one need to collect the data at multiple wavelengths, as a single measurement may have uncertainty of $\pm 2\pi$. However, quantification of spin rotation is more difficult if the fields are arbitrarily directed and not aligned perpendicular to the spin orientation.

Ramsey's technique of separated oscillatory fields, originally introduced for molecular beam resonance, has also been adopted for polarized neutron imaging. Two $\pi/2$ phase-locked spin flippers, oscillating at some frequency (ω), positioned in a homogeneous magnetic field region with the field strength B, flip the spins of a monochromatic, polarized neutron beam twice non-adiabatically. The neutron spin between the flippers precess with Larmor frequency (ω_0) in the plane perpendicular to the continuous magnetic field. After passing through the second flipper, neutrons pass through spin analyser before being detected by a two-dimensional area detector.

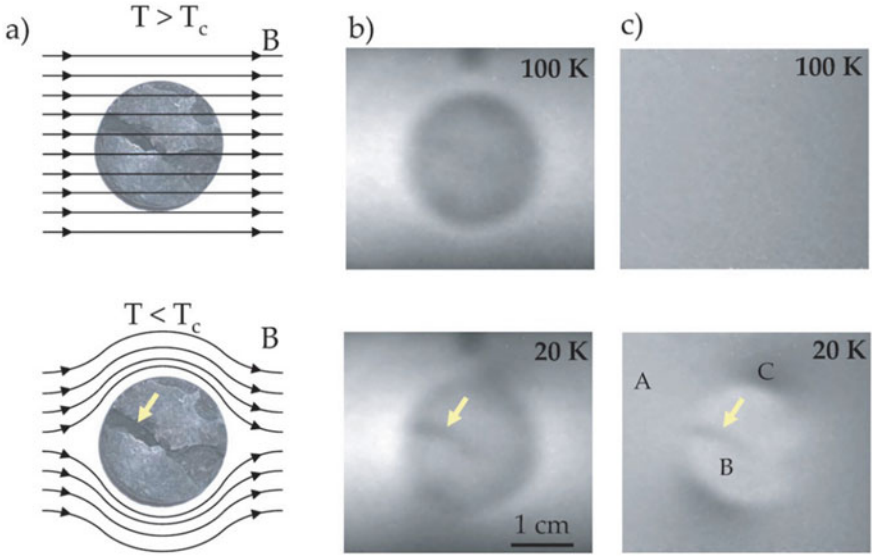

Fig. 1.12 Images of the magnetic field due to the Meissner effect in a YBCO pellet (superconducting) above and below the critical temperature ($Tc = 90$ K), displaying **a** schematic diagrams, **b** raw (unnormalized) radiographs and **c** radiographs normalized to a reference image. The reference was an image of the sample in zero field at 100 K. The arrow indicates a region where expulsion of the field is incomplete [28]

By scanning the frequency (ω) of the oscillating magnetic fields close to Larmor resonance (ω_0) and measuring the consequent spin polarization yields a so-called Ramsey oscillation pattern. By fitting these Ramsey patterns, a phase change at each pixel is obtained. Figure 1.13 shows an example of absorption and spin phase image using the proposed approach.

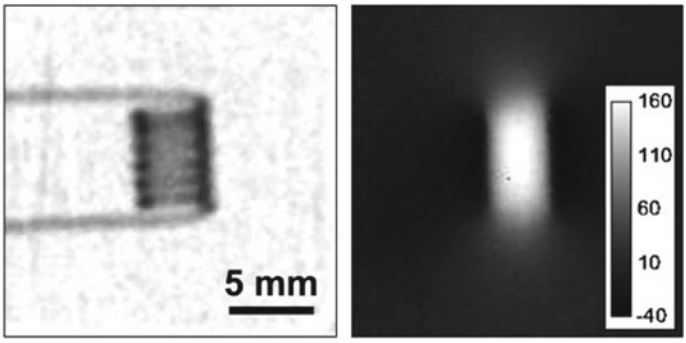

Fig. 1.13 **Left**: Absorption image of a 0.8-mm-thick copper wire coil with six windings, a length of 7 mm, and an inner diameter of 3 mm. **Right**: Image of the magnetic field produced by this coil with a current of 3 A. (reproduced from [29] © 2009 with permission from Elsevier)

The problem of precession of neutron spin in the external and sample fields can be corrected by a second, counter-oriented field to address the shortcomings of Ramsey spin-based phase imaging. This enables spin-echo polarized neutron imaging, in which neutron spin is precessed in the pre-sample flight route, transmitted through the sample and then precessed again in the post-sample flight path. A neutron spin analyser is used to monitor the number of spin precessions. This allows the use of low monochromatized neutron beam and quantification of field integrals which are also simplified due to spin-echo effects.

1.5.4 Bragg Edge Imaging

Bragg edge imaging, a wavelength-dependent neutron radiography, is a non-destructive characterization method and is used to obtain quantitative spatial information on the atomic and internal structures of bulk matter. In the traditional neutron diffraction experiments, Bragg diffraction peaks can be seen at wavelengths where the Bragg conditions are satisfied. It may be noted that the instruments at reactor sources record diffraction patterns as a function of diffraction angle, while pulsed sources record diffraction patterns as a function of wavelength at fixed diffraction angles. On the contrary, Bragg edge imaging is carried out in transmission mode and spectrum is recorded as a function of wavelength, and recorded spectrum displays abrupt changes in the transmission called Bragg edges. Bragg edges in the transmission spectrum are the characteristic of Bragg scattering from polycrystalline materials. For a specific crystal lattice family (hkl), with lattice spacing d_{hkl}, the scattering angle increases with the wavelength up to $\lambda = 2d_{\mathrm{hkl}} \sin(\theta) = 2d_{\mathrm{hkl}} \sin\ (\pi/2)$. The Bragg condition is no longer satisfied beyond this wavelength, resulting in a dramatic drop in the material's attenuation, known as the Bragg edge. Thus, the characterization of crystalline properties of materials such as lattice strains or phase fractions is possible, thanks to the analysis of the Bragg edges. Figure 1.14 shows an example of (110) lattice strain variation as obtained through the Bragg edge imaging technique under in situ load conditions.

Another useful imaging modality called white beam neutron topography, which is based on Bragg diffraction, has been used for visualization of defects such as dislocations and twins present within the crystal volume. In the neutron topography, the image of the object is recorded via Bragg diffraction by the object out of the incident beam, rather than the differential absorption of neutrons along the beam path, as in traditional transmission radiography. Neutron topography has proved useful for monitoring crystal growth and crystal quality and visualizing defects in many different crystalline materials. One can use both monochromatic and polychromatic neutron beam to carry out the measurements. Anti-ferromagnetic domains, chirality domains and other anti-ferromagnetic domains have all benefited from polarized neutron topography [31].

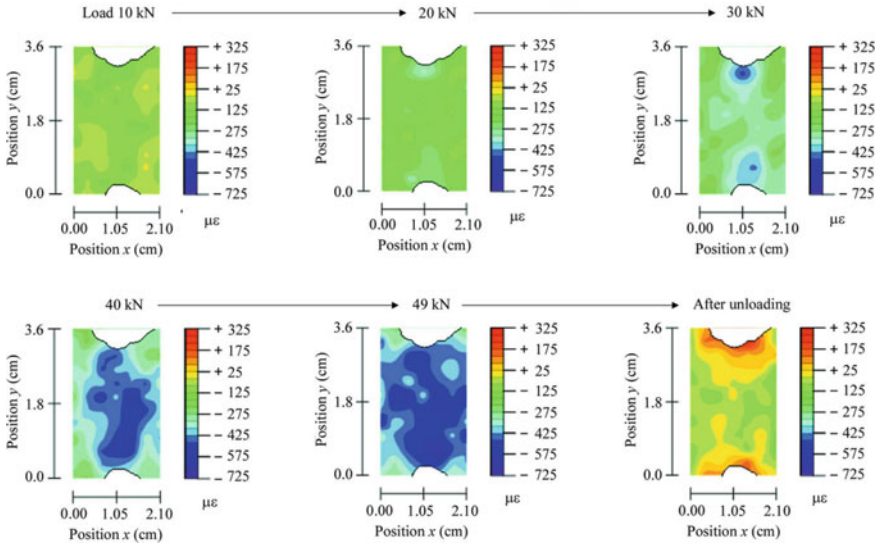

Fig. 1.14 In situ measurement of 110 lattice strain mapping during deformation due to external load using Bragg edge imaging in a 5-mm-thick ferritic steel plate (reproduced with permission of the International Union of Crystallography [30])

1.6 X-ray Versus Neutron Imaging

Soon after Wilhelm Rontgen discovered X-rays, it started being widely used in medical diagnostics and industrial non-destructive testing, due to the larger penetration depth of new radiation. Neutrons being charge neutral have even larger penetration depths in most materials and therefore offer a unique way to increase the probing depths. All traditional radiography technologies (such as X-ray or neutron) work on the same principle: radiation is attenuated when it passes through matter. The specimen is positioned in the path of the incoming incident radiation beam. After passing through sample, the unattenuated beam is detected at the detector, which records the fraction of the initial intensity transmitted by each point in the object. Inhomogeneities in the object or an internal defect (e.g. void, crack, porosity or inclusion) will manifest as a change in intensity of incident beam as recorded by the detector. Defect detection in conventional radiography is thus based on observing differences in radiation intensity as it passes through the object under examination. This occurs as in accordance with the Beer–Lambert law, which can be expressed more precisely as follows:

$$I = I_0 \mathrm{e}^{-\int \mu \mathrm{d}l} \tag{1.24}$$

where I_0 and I are the incident and attenuated intensities, respectively, μ is the linear attenuation coefficient of the material (combining the interaction cross section and nuclear density), and dl is the path length through the sample.

As shown in Eq. (1.24), radiography provides integrated information about the amount of attenuation, which cannot be split into contributions from distinct elements and the amount of material corresponding to the path length. This is standard "inverse problem", though ill-posed, can be solved using the concept of radon transform and Fourier back projection techniques or through iterative reconstruction methods and is called "tomography". As a result, in order to obtain the distribution of the attenuation map, multiple radiographs (projections) for different angular orientations must be collected. The tomographic scan produces three-dimensional spatially resolved images (i.e. volumetric data) that show the distribution of attenuation coefficients in the sample volume.

Regardless of the type of radiation used, the broad strokes of the imaging method are the same. A source emits the radiation, which passes through a collimator. The collimator filters and restricts the passage of radiation ensuring that only parallel beams pass through. Beam collimation improves image quality, resulting in a sharper and more detailed image. Once the beam is collimated, it collides with the object to be imaged. However, there is one important difference: the attenuation X-ray cross section varies linearly with atomic number, whereas it is essentially random for neutrons (Fig. 1.15). This is attributed to the very different nature of their interaction within the matter: X-ray interacts primarily with electron cloud while neutron interacts with nucleus. Figure 1.16 shows the contrasting behaviour of X-ray and neutron radiographic imaging. The flower being rich in hydrogenous matter offers much better attenuation to neutrons as compared to the X-rays. Therefore, one can see the flower in neutron radiography even if hidden in a lead cask of 5 mm thickness. On the other hand, X-rays interact mostly with the lead matrix of cask, and flower

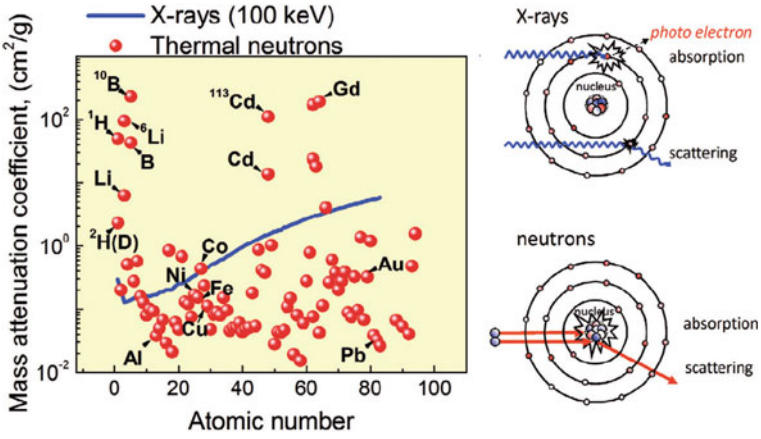

Fig. 1.15 Mass attenuation coefficient of thermal neutrons and 100 keV X-rays (reproduced from [32] © 2011, with permission from Elsevier)

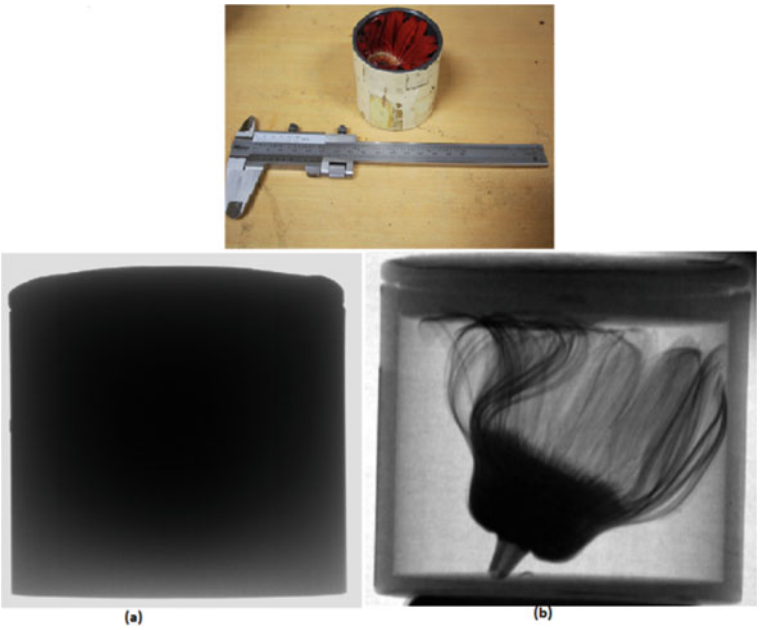

Fig. 1.16 Comparison of (**a**) X-ray and (**b**) neutron radiographs showing the sensitivity of neutron to hydrogeneous materials

being rich in hydrogenous matter, offers very little attenuation to X-rays and hence not visible in X-ray radiograph.

X-rays can undergo elastic or inelastic scattering while passing through a material medium. Photoelectric absorption and Compton scattering are the two major modes of inelastic scattering of X-rays. This results in loss of intensity in the forward direction, i.e. removal of photons along the beam path and hence both are treated as absorption phenomenon. In the elastic scattering, the energy of X-ray photons remains unchanged by the scattering event. The only effect of the scattering is a change of direction which depends upon parameters such as average electron density distribution and incident wave vector and contributes only to the phase shift. X-rays are electromagnetic waves, and their interaction with the matter is governed by a complex refractive index:

$$\begin{aligned} n &= 1 - \delta - i\beta \\ &= 1 - \frac{n_a r_e \lambda^2}{2\pi}(f_1 + i f_2) \end{aligned} \tag{1.25}$$

where $\delta = \frac{n_a r_e \lambda^2}{2\pi} f_1$ and $\beta = \frac{n_a r_e \lambda^2}{2\pi} f_2$.

The quantity $f = f_1 + i f_2$ is known as the effective atomic scattering factor. $f_1 \propto Z$ is responsible for the phase shift and is dependent upon the number of

electrons, and $f_2 \propto \mu$ is responsible for the attenuation. In the energy regime where the photoelectric effect dominates, $\mu \propto Z^4$, implying that the higher the atomic number, the higher is the attenuation contrast.

It may be briefly recalled that quantum mechanics permits the neutron to be treated as a wave and hence corresponding wave equation is given by the Schrodinger equation. Taking a cue from the above treatment, one can compare neutron and X-ray interaction through the following definition of a complex refractive index for neutron:

$$\begin{aligned} n &= 1 - \delta - i\beta \\ &= 1 - \frac{\lambda^2 N}{2\pi}\sqrt{b_c^2 - \left(\frac{\sigma_r}{2\lambda}\right)^2} - i\frac{\sigma_r N\lambda}{4\pi} \end{aligned} \tag{1.26}$$

Thus, we can see that this approach of defining the refractive index is very similar to that of X-ray imaging. Thus, one can say that phase contrast imaging exploits the real part of the refractive index ($1-\delta$) while neutron radiography exploits the imaginary part (β). In comparison with the refractive index of X-rays, which is generally slightly less than unity, the refractive index of neutrons can either be greater than or less than unity. This is due to the fact that the coherent scattering length for neutrons can be positive or negative. Moreover as shown previously, the nuclear scattering lengths vary in a very random way, and therefore, absorption cross section does not exhibit any systemic behaviour.

The resolution and penetrability of X-rays and neutrons are quite different. Neutrons are more penetrative; however, they have a lower resolution (~100 μm) and imaging speed (~s). However, neutron and X-ray images complement each other perfectly. Therefore, it is a good idea to probe the sample using both X-ray and neutron and carry out correlative X-ray and neutron imaging studies imaging. Figure 1.17 shows comparison of X-ray and neutron tomography and brings out their respective importance in non-destructive investigation of energy storage device such as batteries. As seen from these tomography data, structural details are readily visible in X-rays, while neutrons offer much better understanding of water kinetics of the chemical reaction. As shown in Fig. 1.18, correlative X-ray and neutron imaging is a powerful tool in non-destructive analysis where both structural and chemical information is needed. X-ray computed tomography enables identification of mechanical degradation processes while neutron tomography is useful in understanding of lithium diffusion process. This method is extremely useful because X-ray tomography provides mechanical information about the electrodes, such as structure and volume, while neutron tomography provides electro-chemical information, such as Li-ion transportation and intercalation, electrolyte consumption and wettability, among other things.

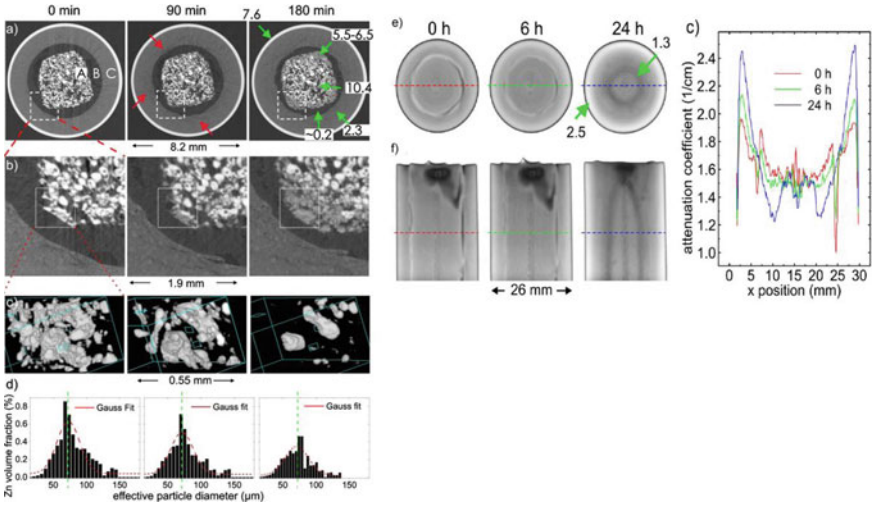

Fig. 1.17 Comparison of X-ray and neutron radiographs showing internal details of conventional battery. X-rays tomography shows up the structure details (**a–d**), while water migration is quite clear in neutron imaging (**e–f**) (reproduced from [33] with permission from Copyright © 2007 American Institute of Physics)

1.7 Summary

Neutrons, as free chargeless and spin 1/2 particles, have properties that make them unique tool to probe into a wide variety of materials. Neutron-based techniques complement a number of other diffraction (X-rays, electrons) and spectroscopy-based experimental methods. Table 1.3 summarizes a comparison of some properties of neutron and X-rays. The large mean free of neutron in most of materials and their ability to reveal the internal structure and distinguish between isotopes has made them an important tool in scientific and industrial research. Advances in instrumentation and refinements in the experimental techniques in the last two decades have led to the development of new neutron imaging modalities. Several new neutron imaging facilities with better neutron fluence and brilliance are under development. In particular, in recent years neutron imaging has been developed into powerful alternative to X-ray imaging techniques to studying the internal structure of the matter and their magnetic properties. The advanced methods phase contrast imaging, Bragg edge imaging and polarized neutron imaging provide more detailed information, e.g. visualization of the crystalline structure, magnetic domain walls or the crystal orientation. The neutron imaging techniques are also being used by industrial users, thereby expanding the scope of neutron imaging and making instruments available to the greater benefit of community.

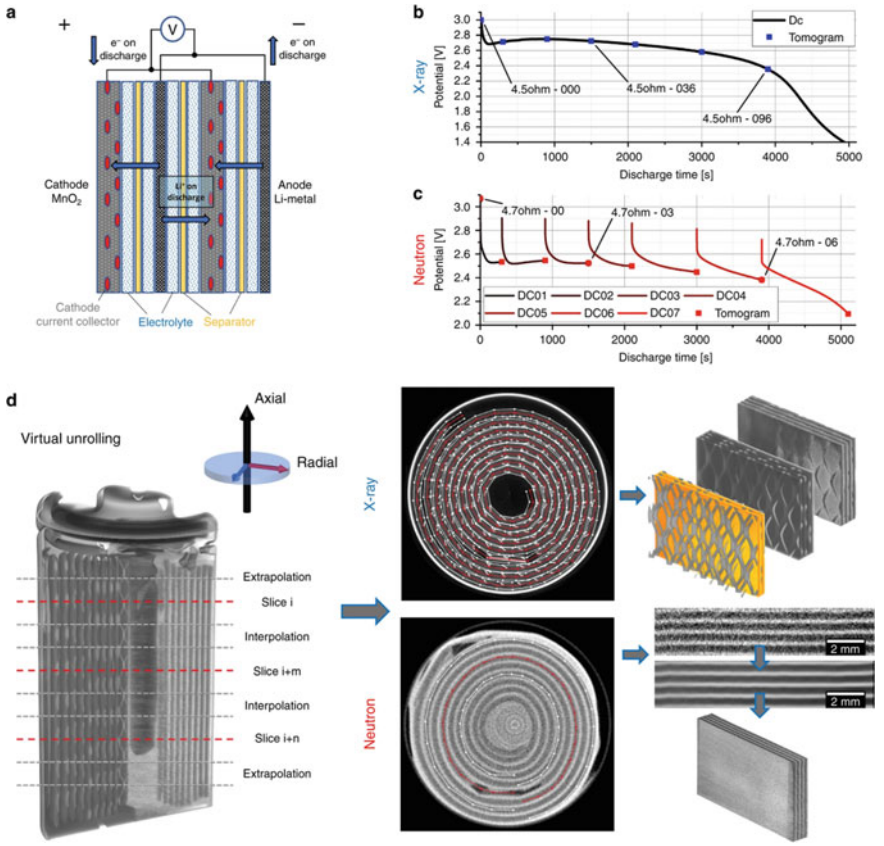

Fig. 1.18 **a** Schematic of Li/MnO2 CR2 primary cell from duracell **b** shows the constant resistance discharge curve for the CR2 cell, **c** depicts the constant resistance discharge curve, **d** shows reconstructed tomograms from neutron and X-ray CT scans, as well as examples of sections extracted after virtual unrolling of the reconstructions. The nickel current collecting mesh, which appears brighter than the Li_xMnO_2 active electrode material, is clearly visible in the X-ray images (reproduced from [34] with permission from Springer Nature)

Table 1.3 Comparison of X-rays and neutron's properties

Feature	X-rays	Neutrons
Free space velocity and energy	$V(\text{m/s}) = c$	$V(\text{m/s}) = 437.39\sqrt{E(\text{meV})}$
Wavelength and energy	$\lambda(\text{A}) = 12.4/E(\text{keV})$	$\lambda(\text{A}) = 9.05/\sqrt{E(\text{meV})}$
Wave equation	$\nabla^2 E(\vec{r}) + \frac{\omega^2}{c^2} E(\vec{r}) = 0$ $E(r,t) = A\text{e}^{i\left(\vec{k}\cdot\vec{r}-\omega t\right)}$	$\nabla^2 \psi(\vec{r}) + \frac{2mE}{\hbar^2} \psi(\vec{r}) = 0$ $\psi(\vec{r},t) = A\text{e}^{i\left(\vec{k}\cdot\vec{r}-Et/\hbar\right)}$
Dispersion relation	$k^2 = \frac{\omega^2}{c^2}$	$k^2 = \frac{2mE}{\hbar^2}$
Phase velocity	$v_{\text{ph}} = \frac{\omega}{k} = c$ (wave packet profile is constant)	$v_{\text{ph}} = \frac{\omega}{v/c} > c$ (wave packet profile changes with time)

References

1. https://mappingignorance.org/2020/06/10/neutron-sciences-as-an-essential-tool-to-develop-materials-for-a-better-life/. Accessed on 15 July 2021
2. Bell RE, Elliott LG (1948) Gamma-rays from the reaction ^{1}H(n, γ)D2 and the binding energy of the deuteron. Phys Rev 74(10):1552–1553
3. Bell RE, Elliott LG (1950) Gamma-rays from the reaction ^{1}H(n, γ)D2 and the binding energy of the deuteron. Phys Rev 79(2):282–285
4. Shull CG, Billman KW, Wedgwood FA (1967) Experimental limit for the neutron charge. Phys Rev 153(5):1415–1422
5. Olive KA (2014) Review of particle physics. Chin Phys C 38(9):090001
6. Alvarez LW, Bloch F (1940) A quantitative determination of the neutron moment in absolute nuclear magnetons. Phys Rev 57(2):111–122
7. Perkins DH (1982) Introduction to high energy physics. Addison-Wesley Advanced Book Program/World Science Division
8. Bég MAB, Lee BW, Pais A (1964) SU(6) and electromagnetic interactions. Phys Rev Lett 13(16):514–517
9. Sherwood JE, Stephenson TE, Bernstein S (1954) Stern-gerlach experiment on polarized neutrons. Phys Rev 96(6):1546–1548
10. Hughes DJ, Burgy MT (1949) Reflection and polarization of neutrons by magnetized mirrors. Phys Rev 76(9):1413–1414
11. Wietfeldt FE, Greene GL (2011) Colloquium: the neutron lifetime. Rev Mod Phys 83(4):1173–1192
12. Yue AT et al (2013) Improved determination of the neutron lifetime. Phys Rev Lett 111(22):222501
13. Particle Data Group (2018) Review of particle physics. Phys Rev D 98(3):030001
14. Schlenker M, Baruchel J (1986) Neutron topography: a review. Physica B+C 137(1):309–319
15. Luschikov VI et al (1969) Observation of ultracold neutrons. Sov Phys—JETP Lett 9:23
16. Zeldovich YaB (1959) Storage of cold neutrons. Sov Phys—JETP 9:1389
17. https://www.psi.ch/en/niag/neutron-physics. Accessed on 15 Sept 2021
18. https://www.nuclear-power.com/nuclear-power/reactor-physics/atomic-nuclear-physics/fundamental-particles/neutron/neutron-energy/. Accessed on 15 Sept 2021

19. Carpenter J, Loong C (2015) Elements of slow-neutron scattering: basics, techniques, and applications. Cambridge University Press, Cambridge. https://doi.org/10.1017/CBO9781139029315
20. Ederth T (2018) Neutrons for scattering: what they are, where to get them, and how to deal with-them. EPJ Web Conf 188:01002. https://doi.org/10.1051/epjconf/201818801002. Accessed on 25 August 2021
21. http://cds.cern.ch/record/1514295/plots. Accessed on 27 July 2021
22. Kardjilov N, Manke I, Woracek R, Hilger A, Banhart J (2018) Advances in neutron imaging. Mater Today 21:652–672
23. Shukla M, Roy T, Kashyap Y et al (2018) Development of neutron imaging beamline for NDT applications at Dhruva reactor, India. Nucl Instrum Methods Phys Res Sect A 889:63–68
24. Saito Y, Mishima K, Tobita Y, Suzuki T, Matsubayashi M (2004) Velocity field measurement in gas–liquid metal two-phase flow with use of PIV and neutron radiography techniques. Appl Radiat Isot 61:683–691
25. Song B, Dhiman I, Carothers JC, Veith GM, Liu J, Bilheux HZ, Huq A (2019) Dynamic lithium distribution upon dendrite growth and shorting revealed by operando neutron imaging. ACS Energy Lett 4(10):2402–2408
26. Jacobson DL, Allman BE, McMahon PJ, Nugent KA, Paganin D, Arif M, Werner SA (2004) Thermal and cold neutron phase-contrast radiography. Appl Radiat Isot 61:547–550
27. Pfeiffer F, Grünzweig C, Bunk O, Frei G, Lehmann E, David C (2006) Neutron phase imaging and tomography. Phys Rev Lett 96:215505
28. Dawson M et al (2009) Imaging with polarized neutrons. New J Phys 11:043013. https://doi.org/10.1088/1367-2630/11/4/043013. Accessed on 25 August 2021
29. Piegsa FM, van den Brandt B, Hautle P, Konter JA (2009) A compact neutron Ramsey resonance apparatus for polarised neutron radiography. Nucl Instrum Methods Phys Res Sect A 605:5–8
30. Iwase et al (2012) In situ lattice strain mapping during tensile loading using the neutron transmission and diffraction methods. J Appl Cryst 45:113–118
31. Baruchel J, Schlenker M, Palmer SB (1990) Neutron diffraction topographic investigations of "exotic" magneticdomains. Nondestr Test Eval 5(5–6):349–367. https://doi.org/10.1080/02780899008952978
32. Kardjilov N, Manke I, Hilger A, Strobl M, Banhart J (2011) Neutron imaging in materials science. Mater Today 14:248–256
33. Mankea I, Banhart J et al (2007) In situ investigation of the discharge of alkaline Zn–MnO2 batteries with synchrotron X-ray and neutron tomographies. Appl Phys Lett 90:214102
34. Ziesche RF, Arlt T, Finegan DP et al (2020) 4D imaging of lithium-batteries using correlative neutron and X-ray tomography with a virtual unrolling technique. Nat Commun 11:777